Parametric instabilities of microcavity polaritons in a periodic potential

A. V. Gorbach and D. V. Skryabin
Centre for Photonics and Photonic Materials, Department of Physics, University of Bath, Bath BA27AY, United Kingdom
(Received 25 May 2010; published 13 September 2010)

We analyze parametric instabilities of microcavity polartions in the presence of one-dimensional periodic potentials. Instabilities appear in a certain window of pump momentum orientations with respect to the potential so that the momentum projection onto the direction of periodicity is large enough. Ring-shaped domains of parametrically amplified perturbations form a periodic chain in momentum space. Independently from the orientation of the pump momentum, the chain maintains its orientation along the direction of periodicity of the system. In the physical space the amplified structures emerge as stripes modulated along the direction of periodicity and of finite width in the orthogonal direction.

DOI: 10.1103/PhysRevB.82.125313 PACS number(s): 42.65.Yj, 42.65.Sf, 71.36.+c

I. INTRODUCTION

Polaritons existing due to strong coupling between photons and excitons in semiconductor microcavities[1,2] have attracted much attention following recent successful demonstration of their nonequilibrium condensation using incoherent[3,4] and coherent[5,6] pumping. Among peculiar features of polaritons in the strong-coupling regime are ultrafast and strong nonlinearity provided by the repulsive interaction of excitons and the unusual shape of the lower dispersion branch having the inflection point where the effective polariton mass changes sign. Combination of these features leads to a variety of effects not seen in the microcavities operating in the weak-coupling regime.[7] In particular, the specific shape of the dispersion makes it possible to satisfy resonance conditions for parametric scattering of a degenerate pair of pump polaritons into the signal and idler ones.[8] Both parametric amplification of the seeded signal[9,10] and spontaneous polariton emission through parametric (modulational) instability[5,6,9] have been experimentally observed in microcavities pumped in a vicinity of the inflection point. Comprehensive theoretical investigation of these processes can be found, e.g., in Ref. 11.

A well known possibility to control dispersion and hence the sign of effective mass is by means of periodic potentials. Recent studies of parametric processes in photonic crystal cavities have revealed such effects as inhibition of parametric instability by the photonic band gap,[12,13] on one hand, and instabilities induced by the periodic potential,[13] on the other. Existence of various localized structures due to inverted effective mass have been revealed in photonic crystal cavities[14,15] and recently in polariton cavities.[16] Coherent excitation of different periodic polariton states, polariton lattices, has been experimentally realized using either acoustic modulation[18] or mirrors with a pattern of metal stripes.[17] The former approach is more flexible since both amplitude and period of the potential are readily controlled.[18,19]

In this work we discuss instabilities of polaritons induced by the presence of one-dimensional periodic potentials. Periodicity of the system strongly modifies dispersion of small amplitude perturbations, Bogolyubov spectrum, in the corresponding direction. For weak potentials this modification can be understood as folding of the spectrum of the homogeneous system into the first Brillouin zone. We demonstrate, that for different orientations of the pump momentum, the folding leads to crossings of branches of forward- and backward-propagating polaritons having either the same or opposite signs of energy. Taking into account potential-induced interactions, the former leads to the avoided anticrossing in the spectrum, while the latter to the parametric instabilities.

II. MODEL AND POLARITON LATTICES

A well accepted dimensionless mean-field model describing strong coupling of excitons and photons in semiconductor microcavities is[2,20]

$$\partial_t E - i\nabla^2 E + [\gamma_{ph} - iU(y)]E = i\Psi + E_p e^{i\vec{k}_p\vec{r} - i\delta_p t}, \quad (1)$$

$$\partial_t \Psi + [\gamma_e - iW(y)]\Psi + i|\Psi|^2\Psi = iE, \quad (2)$$

where E is the slowly varying amplitude of the intracavity electric field and Ψ is the amplitude of the coherent excitons. $\nabla^2 \equiv \partial_x^2 + \partial_y^2$, $\vec{r} = \vec{i}x + \vec{j}y$, where (x,y) is the microcavity plane. We assume that the cavity is in resonance with excitons. δ_p is the detuning of the pump beam E_p from the resonance. $\vec{k}_p = k_p(\vec{i}\cos\theta + \vec{j}\sin\theta)$ is the in-plane pump momentum with $k_p = 0$ corresponding to the normal incidence. Polarization of the pump is assumed parallel to the cavity plane so that no change in the polarization state happens when the angle of incidence is varied. Exciton interaction induced, i.e., nonlinear, coupling between orthogonal polarizations is disregarded. γ_{ph} and γ_e are the damping parameters for photons and excitons, respectively. The normalization of equations is described in details in Ref. 20. By varying the Rabi energy between 1 and 10 meV we find that one unit of time varies between 1 and 0.1 ps and one unit of x and y is between 1 and 0.3 μm.

$U(y)$ and $W(y)$ are the one-dimensional periodic potentials, which account for modulations of the cavity and exciton resonances, respectively. For the case of acoustic modulation, and neglecting the relatively slow motion of phonons, both potentials have similar strength and can be approximated as[18]

$$U(y) = U_0 \cos(2\pi y/L), \quad (3)$$

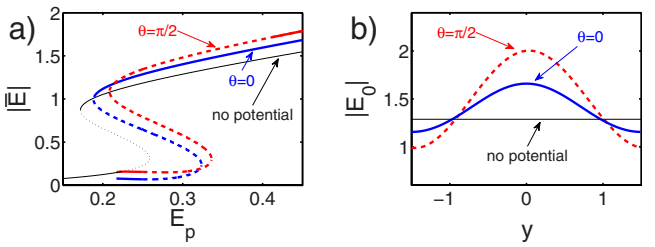

FIG. 1. (Color online) Polariton lattices. (a) Average amplitude $\bar{E}=1/L\int dy E_0(y)$ of the lattice solutions as a function of E_p: $\theta=0$ and $\theta=\pi/2$. $U_0=W_0=0.75$, $\delta_p=-0.3$, $k_p=0.8$, and $\gamma_{ph}=\gamma_e=0.1$. Solution for the no potential case $U_0=W_0=0$ is plotted with thin black lines. Solid/dashed lines correspond to stable/unstable branches. (b) Profiles of the lattice solutions for $E_p=0.3$, $\theta=0$ (blue solid line), $\theta=\pi/2$ (red dashed line), and no potential (thin black line) cases.

$$W(y) = W_0 \cos(2\pi y/L). \tag{4}$$

Typical amplitudes of modulation are on the order of the vacuum Rabi splitting[18] so that $U_0, W_0 \sim 0.5-1$ in our dimensionless units. For the case of potentials created by mirror patterning, only photonic component is modulated: $U_0 \neq 0$ and $W_0=0$. While the ratio between U_0 and W_0 does not qualitatively affect the instabilities discussed, we fix $U_0=W_0$.

Orientation of the pump momentum θ with respect to the periodic potential is critically important for the properties of our system. Below we demonstrate that the potential-induced interactions between polaritons happen in different ways for two principal orientations: along the direction of periodicity y ($\theta=\pi/2$) and along the homogeneous direction x ($\theta=0$).

Stationary polariton lattices are sought in the form $E=E_0(y)e^{i\vec{k}_p\vec{r}-i\delta_p t}$, $\Psi=\Psi_0(y)e^{i\vec{k}_p\vec{r}-i\delta_p t}$, E_0 and Ψ_0 satisfy

$$\partial_y^2 E_0 + i2k_p \sin\theta \partial_y E_0 + [\delta_p - k_p^2 + U + i\gamma_{ph}]E_0 = -\Psi_0 + iE_p, \tag{5}$$

$$[\delta_p + W + i\gamma_e]\Psi_0 - |\Psi_0|^2\Psi_0 = -E_0. \tag{6}$$

This system is solved numerically on the interval $y \in [-L/2, L/2]$ with periodic boundary conditions, by discretizing y dimension and applying Newton-Raphson iterations. The lattice solutions found are shown in Fig. 1 and discussed below.

According to the common experimental conditions,[5,6] we choose the pump frequency within the lower polariton branch, $-1<\delta_p<0$. The pump momentum k_p is taken to be slightly below the inflection point $k_p<k_{cr}\approx 0.9$. For such choice of parameters, the stationary solution in the no potential case ($U_0=W_0=0$) has three branches (S-shape bistability), see thin black curve in Fig. 1(a), with the upper branch being always stable (no parametric instability). Average amplitudes of the polariton lattices are plotted in Fig. 1(a) for the two principal orientations of the pump momentum. The corresponding lattice profiles for the upper branch of the bistability loop are shown in Fig. 1(b). While the bistability is preserved in both cases, the upper branch becomes unstable within a large window of E_p for the pump momentum oriented along the direction of periodicity ($\theta=\pi/2$). As we demonstrate in the following sections, this instability is caused by parametric interactions between forward- and backward-propagating perturbations, and leads to growth of periodic patterns.

III. STABILITY ANALYSIS

To analyze stability of polariton lattices we consider small perturbations to the stationary solution $E_0(y), \Psi_0(y)$: $E=[E_0(y)+e(x,y,t)]e^{i\vec{k}_p\vec{r}-i\delta_p t}$, $\Psi=[\Psi_0(y)+\psi(x,y,t)]e^{i\vec{k}_p\vec{r}-i\delta_p t}$, and linearize the resulting equations for e, ψ. The resulting system can be written as

$$i\partial_t \mathbf{a} = \hat{\eta}\frac{\delta H}{\delta \mathbf{a}^*} - i\hat{\Gamma}\mathbf{a}, \tag{7}$$

where

$$\mathbf{a} = [e, \psi, e^*, \psi^*]^T,$$

$$\delta H/\delta \mathbf{a}^* = [\delta H/\delta e^*, \delta H/\delta \psi^*, \delta H/\delta e, \delta H/\delta \psi]^T,$$

$$\hat{\eta} = \begin{bmatrix} -1 & 0 & 0 & 0 \\ 0 & -1 & 0 & 0 \\ 0 & 0 & 1 & 0 \\ 0 & 0 & 0 & 1 \end{bmatrix}, \quad \hat{\Gamma} = \begin{bmatrix} \gamma_{ph} & 0 & 0 & 0 \\ 0 & \gamma_e & 0 & 0 \\ 0 & 0 & \gamma_{ph} & 0 \\ 0 & 0 & 0 & \gamma_e \end{bmatrix}, \tag{8}$$

and H is the Bogolyubov energy functional,

$$H = \int\int dxdy \Big\{ -|\nabla e|^2 - i\vec{k}_p(e\nabla e^* - e^*\nabla e) + (\Delta_{ph} + U - k_0^2) \times |e|^2 + (\Delta_e + W - 2|\Psi_0|^2)|\psi|^2 + \psi e^* + \psi^* e - \frac{1}{2}\Psi_0^2(\psi^*)^2 - \frac{1}{2}(\Psi_0^*)^2\psi^2 \Big\}. \tag{9}$$

Since all the coefficients in Eq. (9) are periodic in y, we can apply the Floquet-Bloch theorem. Thus we expand perturbations into Bloch modes along y and into plane waves along x direction,

$$f(\vec{r},t) = \int_{-\infty}^{+\infty} d\kappa \int_{-\pi/L}^{\pi/L} dq_B [f_i(y)e^{i\kappa x + iq_B y - i\delta t + \lambda t} + f_s^*(y)e^{-i\kappa x - iq_B y + i\delta t + \lambda t}], \tag{10}$$

where $f_{s,i}=e_{s,i}, \psi_{s,i}$ are periodic in y with the period L, q_B is the quasimomentum along the direction of periodicity, κ is the momentum along the homogeneous direction. λ and δ are real and represent the sidebands growth rates and frequencies, respectively. They are determined from the eigenvalue problem,

$$(\delta + i\lambda)\mathbf{a}_B = (\hat{\eta}\hat{M} - i\hat{\Gamma})\mathbf{a}_B, \tag{11}$$

where $\mathbf{a}_B=[e_i, \psi_i, e_s, \psi_s]^T$ and

$$\hat{M} = \begin{bmatrix} \mathcal{H}_e - D_e & 1 & 0 & 0 \\ 1 & \mathcal{H}_q & 0 & -\Psi_0^2 \\ 0 & 0 & \mathcal{H}_e + D_e & 1 \\ 0 & -(\Psi_0^2)^* & 1 & \mathcal{H}_q \end{bmatrix}, \tag{12}$$

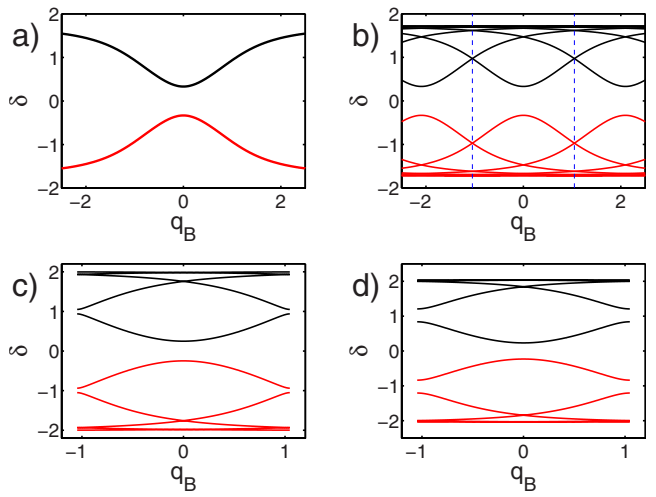

FIG. 2. (Color online) Bogolyubov spectrum for the case of pump momentum oriented along the homogeneous direction ($\theta=0$). (a) Spectrum of the homogeneous system, only two closest to zero branches are shown. Black/red curves correspond to branches with positive/negative Krein signatures. (b) Schematic folding of the spectrum to the first Brillouin zone (boundaries are indicated by dashed vertical lines) in the limit $U_0, W_0 \to 0$, $L=3$. [(c) and (d)] Spectra of periodical system with $U_0=W_0=0.25$ and $U_0=W_0=0.75$, respectively. All figures correspond to the pump parameters $E_p=0.3$ and $k_p=0.8$.

$$\mathcal{H}_e = \partial_y^2 + i2q_B\partial_y + \delta_p - k_0^2 - \kappa^2 - q_B^2 + U(y), \tag{13}$$

$$\mathcal{H}_q = \delta_p + W(y) - 2|\Psi_0|^2, \tag{14}$$

$$D_e = 2k_p\{\kappa \cos\theta + q_B \sin\theta - \sin\theta i\partial_y\}. \tag{15}$$

We solve Eq. (11) numerically by discretizing y on the interval $y \in [-L/2, L/2]$ with periodic boundary conditions. According to our definition, any eigenvalue with $\lambda > 0$ corresponds to the unstable perturbation.

The case of a homogeneous system, $U_0=W_0=0$, is formally recovered by taking $L \to 0$. Then $e_{s,i}$ and $\psi_{s,i}$ become constants while the spectrum of eigenvalues $\delta+i\lambda$ consists of two pairs of branches.[11] Within each pair, branches are related by symmetry transformation $\delta(\vec{k}_p+\vec{\kappa}) = -\delta(\vec{k}_p-\vec{\kappa})$, $\vec{\kappa} = \vec{i}\kappa + \vec{j}q_B$. The stable perturbations have opposite signs of the Bogolyubov energy functional H (Krein signature) in the limit of zero dissipation while unstable perturbations carry zero energy. Collision of two eigenvalues with opposite Krein signatures leads to instabilities while approaching of two eigenvalues with the same Krein signature leads to the branch anticrossing.[21] As we illustrate below, this mechanism still applies when small to moderate dissipation effects, $\hat{\Gamma} \neq 0$, are taken into account.

Since periodic potentials strongly modify dispersion along k_y direction, it is instructive to perform first the simplified one-dimensional analysis assuming $\kappa=0$. In this case the entire momentum of perturbations along the grooves of the potential (x coordinate) is given by the corresponding component of the pump momentum $k_p \cos\theta$. Figure 2(a) shows the spectrum of the stable polariton solution (upper branch)

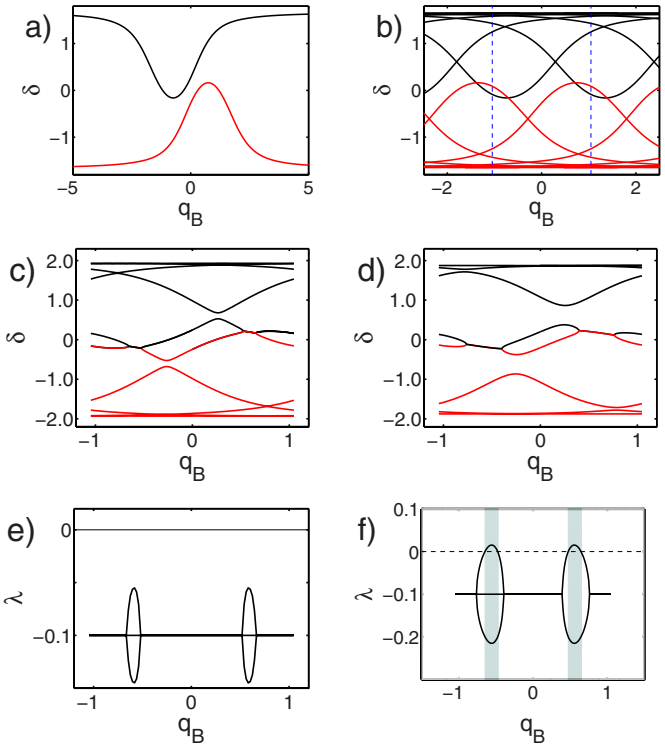

FIG. 3. (Color online) Bogolyubov spectrum for the case of pump momentum oriented along the direction of periodicity ($\theta=\pi/2$). [(a)–(d)] The same as Fig. 2 but for $\theta=\pi/2$. [(e) and (f)] Gain of perturbations corresponding to figures (c) and (d), respectively. Shaded areas indicate range of unstable perturbations ($\lambda > 0$).

in the homogeneous microcavity for the case when pump is tilted along x direction ($\theta=0$). Only two branches closest to zero are shown, the other two are located further away and do not play role in the instabilities discussed below. With the potentials, the spectrum becomes periodic in q_B. In the limit of small $U_0, W_0 \to 0$, its structure can be approximated by plotting replicas of the spectrum of the homogeneous system shifted in q_B by $2\pi n/L$, $n=0, \pm 1, \pm 2, \ldots$, and considering range of quasimomenta within the first Brillouin zone $-\pi/L \leq q_B \leq \pi/L$, see Fig. 2(b). One can see that this folding leads to *intrabranch* intersections of eigenvalues having the same Krein signature (since the same branch is involved) near the edges and center of the Brillouin zone. At each intersection forward- ($\partial\delta/\partial q_B > 0$) and backward-propagating ($\partial\delta/\partial q_B < 0$) perturbations have the same complex eigenvalue $\delta+i\lambda$. For any nonzero amplitudes of the potentials, the periodicity-induced interaction between these perturbations lifts the degeneracy, so that frequencies δ of forward- and backward-propagating perturbations split. This leads to appearance of additional gaps in the spectrum, becoming wider as the potential strength is increased, see Figs. 2(c) and 2(d).

Different scenario occurs when the pump is tilted along y direction ($\theta=\pi/2$), see Fig. 3. Now the two branches of the homogeneous system overlap in δ and are separated in q_B, see Fig. 3(a). As the result, the folding into the first Brillouin zone leads to the *interband* intersections, mixing perturbations with opposite Krein signatures, see Fig. 3(b). For non-

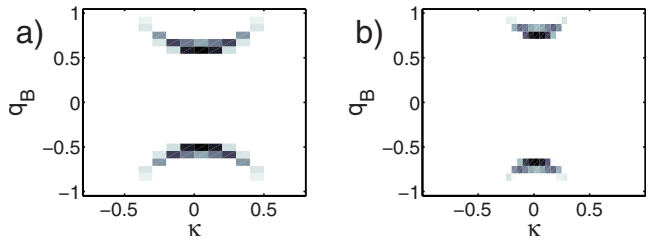

FIG. 4. (Color online) Results of 2D stability analysis. Shaded areas indicate domains of unstable perturbations for E_p=0.3 and pump orientations (a) $\theta=\pi/2$ and (b) $\theta=3\pi/8$. Other parameters are the same as in Fig. 1.

zero U_0 and W_0 such degeneracies are lifted through splitting of imaginary parts λ of complex eigenvalues, see Figs. 3(c) and 3(e). Increasing the strength of potentials, one of the λ's in each pair is pushed above zero, resulting in the instability. Due to the symmetry of the problem, unstable perturbations always appear in pairs $\pm q_B$, with the corresponding detunings from the pump frequency $\pm\delta$. This is typical for parametric processes with $+q_B(-q_B)$ corresponding to the signal (idler) beams. Further increase in U_0 and W_0 leads to wider domains of instabilities, see Figs. 3(d) and 3(f).

When the pump momentum is taken beyond the inflection point, $k_p > k_{cr}$, interband intersections leading to parametric instabilities become possible in the homogeneous system with no potential.[11] In contrast to the above discussed intersections due to the folding, two branches in a vicinity of the crossing point have the same sign of group velocity $\partial\delta/\partial k$ in that case.

Taking into consideration perturbations with all possible $\kappa \neq 0$, we have found that the domains of unstable perturbations in the (κ, q_B) plane are always aligned along the $\kappa=0$ axis with the maximal gain achieved at $\kappa=0$, $q_B \neq 0$, see Fig. 4. Rotating the in-plane pump momentum from $\theta=\pi/2$ to $\theta=0$, the domains gradually shrink and disappear, while they remain centered at $\kappa=0$, cf. Figs 4(a) and 4(b). This is in a sharp contrast with the case of parametric instabilities of polaritons in a homogeneous cavity, where the two domains are always oriented along the direction of the pump momentum,[11] and hence rotate together with θ.

In Fig. 5(a) the maximal gain is plotted as the function of the pump orientation θ. The gain becomes larger with growing y component of the pump momentum, reaching its maximum value at $\theta=\pi/2$. Increase in the pump amplitude with fixed θ suppresses the instability so that polariton lattices

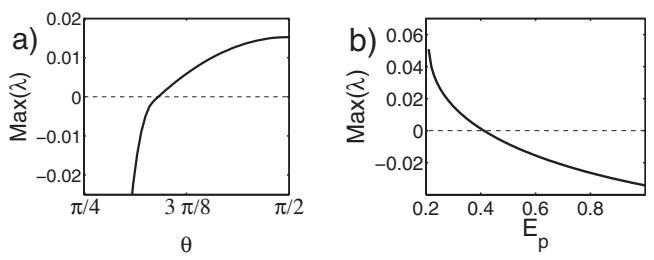

FIG. 5. [(a) and (b)] Maximal perturbation growth rate as functions of the pump tilt for E_p=0.3 and pump amplitude for $\theta=\pi/2$, respectively. Other parameters are the same as in Fig. 1.

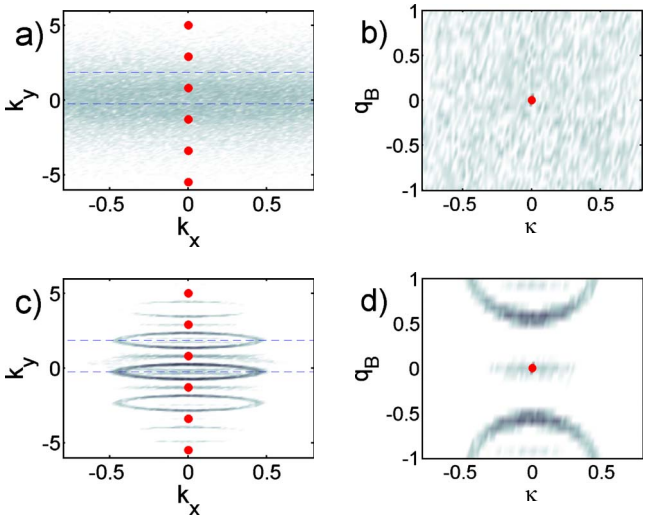

FIG. 6. (Color online) Numerical propagation results: full spectrum (left) and folded to the first Brillouin zone (right) at different times: [(a) and (b)] t=200 and [(c) and (d)] t=500. Dashed horizontal lines indicate boundaries of the first Brillouin zone. Spectrum of the polariton lattice is shown with solid circles. Parameters of the pump and lattice are the same as in Fig. 4(a). Parameters of the seed pulse are: T=2.5, t_0=200, and ϵ=0.01.

become stable far enough from their bistability domain, cf. Figs 1 and 5(b).

IV. DYNAMICAL GROWTH OF PERTURBATIONS

In order to validate our stability analysis and study long time evolution of polariton lattices in the unstable regime, we have performed a series of direct simulations of Eqs. (1) and (2). Parametric instabilities have been triggered by a short input pulse added to the right-hand side of Eq. (1),

$$E_s(\vec{r},t) = \xi(\vec{r})e^{i\vec{k}_0\vec{r}}e^{-(t-t_0)^2/T^2}, \tag{16}$$

where $\xi(\vec{r})$ is a complex function with a random phase, $|\xi(\vec{r})| \equiv \epsilon \ll |E_p|$, $\vec{k}_0$ shifts the momentum so that the spectrum of ξ covers a large area in k space surrounding one of the predicted regions of unstable perturbations, see Figs. 6(a) and 6(b). The initial fields are set to zero, and the seed pulse of duration T is delayed in time by $t_0 \gg T$, permitting the system to relax to the stationary state.

Results of our numerical simulations are summarized in Figs. 6 and 7. Spectrum of the stationary lattice appears in Figs. 6(a) and 6(c) as the periodic grid of points located at $k_x=k_p\cos(\theta)$, $k_y=k_p\sin(\theta)+2\pi n/L$, $n=0,\pm1,\pm2,\ldots$ Subtracting the pump momentum, $\vec{\kappa}=\vec{k}-\vec{k}_p$, and making reduction to the first Brillouin zone, the grid transforms into the single peak at $q_B=\kappa=0$, see Figs. 6(b) and 6(d). The additional seed pulse excites polaritons with momenta distributed almost evenly across the entire first Brillouin zone, see Fig. 6(b). At larger times we observe parametric amplification of polaritons belonging to the chain of rings in the (k_x,k_y) plane, see Fig. 6(c). Rings are centered at the boundaries of the first and higher Brillouin zones, forming a periodic chain along k_y axis. Following reduction to the first Brillouin zone,

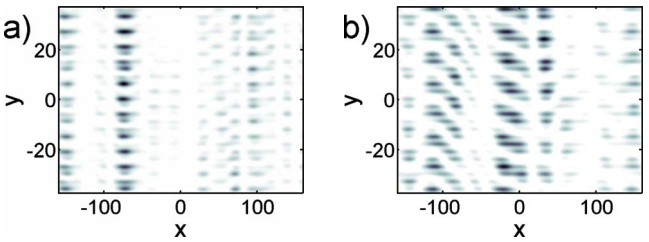

FIG. 7. (Color online) Field intensity patterns following evolution of unstable perturbations. (a) $\theta=\pi/2$ and $t=500$; (b) $\theta=3\pi/8$ and $t=850$. Other parameters as in Fig. 6. Polariton lattice solution E_0 is subtracted in the plots in order to isolate the perturbation field.

Fig. 6(d), rings transform into two arcs, as predicted by our linear stability analysis, cf. Figs 4(a) and 6(d).

The corresponding patterns in the physical plane of the cavity are shown in Fig. 7. Because of the vertical orientation of the rings of instability in the momentum space, the emerging real-space patterns have a pronounced chains of high intensity spots, which are also oriented along the y coordinate, regardless orientation of the pump momentum. The period of modulation of stripes along y direction is defined by the corresponding quasimomentum q_B of unstable perturbations and does not generally coincide with the lattice period. Remarkably, amplified structures usually appear as stripes of finite width along x direction. If $\theta \neq \pi/2$, stripes drift along x direction due to the nonzero corresponding component of the pump momentum, but their width remain practically unchanged over long time intervals. Recently we reported a mechanism of localization of polaritons due to the interplay between diffraction and parametric scattering[22] and formation of one- and two-dimensional (2D) solitons supported by this mechanism. The results of our numerical simulations presented in Fig. 7 indicate a possible existence of similar localized structures in microcavities with periodic potentials.

V. SUMMARY

In summary, we reported parametric instabilities of polariton lattices in microcavities with one-dimensional periodic potentials. Periodicity induces interactions between forward- and backward-propagating polaritons. We found that these interactions happen in different ways depending on the orientation of the pump momentum with respect to the potential. When the pump is tilted along the homogeneous direction of the microcavity, the interaction happens between polaritons with the same sign of the Bogolyubov energy. This leads to the anticrossing of the corresponding bands and no instabilities are generated. On the contrary, when the pump momentum component along the direction of the periodicity of the system is large enough, interactions between polaritons with opposite signs of the energy are allowed. Such interactions lead to the parametric instabilities of the polariton lattices. While orientation of the pump momentum with respect to the potential controls the strength of instabilities, the amplified structures are always modulated along the direction of periodicity of the system.

ACKNOWLEDGMENT

We acknowledge support from the EPSRC under Project No. EP/D079225/1.

[1] C. Weisbuch, M. Nishioka, A. Ishikawa, and Y. Arakawa, Phys. Rev. Lett. **69**, 3314 (1992).
[2] A. Kavokin, J. J. Baumberg, G. Malpuech, and F. P. Laussy, *Microcavities* (Oxford University Press, New York, 2007).
[3] J. Kasprzak *et al.*, Nature (London) **443**, 409 (2006).
[4] R. Balili, V. Hartwell, D. Snoke, L. Pfeiffer, and K. West, Science **316**, 1007 (2007).
[5] R. M. Stevenson, V. N. Astratov, M. S. Skolnick, D. M. Whittaker, M. Emam-Ismail, A. I. Tartakovskii, P. G. Savvidis, J. J. Baumberg, and J. S. Roberts, Phys. Rev. Lett. **85**, 3680 (2000).
[6] J. J. Baumberg, P. G. Savvidis, R. M. Stevenson, A. I. Tartakovskii, M. S. Skolnick, D. M. Whittaker, and J. S. Roberts, Phys. Rev. B **62**, R16247 (2000).
[7] T. Ackemann, W. J. Firth, and G.-L. Oppo, Adv. At., Mol., Opt. Phys. **57**, 323 (2009).
[8] D. M. Whittaker, Phys. Rev. B **63**, 193305 (2001).
[9] R. Houdré, C. Weisbuch, R. P. Stanley, U. Oesterle, and M. Ilegems, Phys. Rev. Lett. **85**, 2793 (2000).
[10] P. G. Savvidis, J. J. Baumberg, R. M. Stevenson, M. S. Skolnick, D. M. Whittaker, and J. S. Roberts, Phys. Rev. Lett. **84**, 1547 (2000).
[11] C. Ciuti and I. Carusotto, Phys. Status Solidi B **242**, 2224 (2005).
[12] D. Gomila, R. Zambrini, and G.-L. Oppo, Phys. Rev. Lett. **92**, 253904 (2004).
[13] N. Marsal, D. Wolfersberger, M. Sciamanna, G. Montemezzani, and D. N. Neshev, Opt. Lett. **33**, 2509 (2008).
[14] A. Yulin, D. Skryabin, and P. Russell, Opt. Express **13**, 3529 (2005).
[15] A. G. Vladimirov, D. V. Skryabin, G. Kozyreff, P. Mandel, and M. Tlidi, Opt. Express **14**, 1 (2006).
[16] A. V. Gorbach, B. A. Malomed, and D. V. Skryabin, Phys. Lett. A **373**, 3024 (2009).
[17] C. W. Lai *et al.*, Nature (London) **450**, 529 (2007).
[18] M. M. de Lima, Jr. and P. V. Santos, Rep. Prog. Phys. **68**, 1639 (2005).
[19] M. M. de Lima, Jr., M. van der Poel, P. V. Santos, and J. M. Hvam, Phys. Rev. Lett. **97**, 045501 (2006).
[20] O. A. Egorov, D. V. Skryabin, A. V. Yulin, and F. Lederer, Phys. Rev. Lett. **102**, 153904 (2009).
[21] D. V. Skryabin, Phys. Rev. E **64**, 055601 (2001); J. Opt. Soc. Am. B **19**, 529 (2002).
[22] O. A. Egorov, A. V. Gorbach, F. Lederer, and D. V. Skryabin, Phys. Rev. Lett. **105**, 073903 (2010).